ELSEVIER

Composites: Part B 33 (2002) 367–381

composites
Part B: engineering

www.elsevier.com/locate/compositesb

Modeling of layered timber beams and ribbed shell frameworks

Kai-Uwe Gliniorz[a], Khalid M. Mosalam[a,*], Julius Natterer[b]

[a]*Department of Civil and Environmental Engineering, University of California, 721 Davis Hall, 94720-1710 Berkeley, CA, USA*
[b]*Swiss Federal Institute of Technology, VD-1015 Lausanne, CH Switzerland*

Received 18 March 2002; accepted 15 May 2002

Abstract

A methodology for modeling multi-layered structures is presented. The formulation is easily utilized in the framework of existing structural analysis programs to compute internal forces and the global and local deformations of multi-layered structural members and systems. The methodology is fully applied and verified for the case of multi-layered timber beams with semi-rigid connections between the layers. The verifications are performed using both static experimentation and detailed computational modeling with linear and nonlinear finite element analyses. Extension to curved members is also included where emphasis is focused on residual stresses due to construction procedures of layered timber arches. Finally, experimental and computational demonstration of the methodology is given from timber ribbed shells where reasonable agreement between model predictions and experiments is illustrated. © 2002 Published by Elsevier Science Ltd.

Keywords: C. Computational modeling; C. Finite element analysis; Orthotropic material

1. Introduction

Shells are a fascinating class of structures from both professional and public perspectives. This type of construction is still in its infancy and therefore requires better understanding of several modeling and design aspects. In the contemporary construction practice, the number of constructed reinforced concrete and steel shells is much higher than that of timber shells. This is attributed to lack of knowledge about the design and construction of timber shells. Ribbed shells in the form of nailed or doweled planks as shown in Fig. 1, are characterized by geometric anisotropy in addition to the inherent material anisotropy of timber. Moreover, such shells present highly statically indeterminate structural systems. This imposes a challenge in the analysis and design of ribbed timber shells.

This paper presents the results of an ongoing research at the chair for timber construction at the Swiss Federal Institute of Technology in Lausanne and more recently at the University of California, Berkeley. A methodology for numerical computation of the deformations and stresses in various timber multi-layer structures is developed. This methodology is developed and verified for layered timber beams and extended to curved members for subsequent utilization in analysis and design of timber ribbed shells. As a direct consequence of this research, the design of such timber structures is benefiting through contributions to Appendix F of Ref. [6]. This appendix describes the composite behavior of plane and curved structural components and systems consisting of several timber layers. It specifies standards for estimating stiffness values for the computations of deformations and internal forces. It is worth mentioning that the presented methodology is also applicable to other layered composite structures.

The paper starts by summarizing the linear elastic computational model of multi-layer beams which includes both stress and deformation computations. This model is intended as a practical solution to the problems involving deformation discontinuities along the joint surfaces of multi-layered structures. Subsequently, the model is applied to a test specimen of a layered timber beam, which was also analyzed using linear and nonlinear finite element analyses and comparisons are included. Extension to curved members is then included where curved layered timber beam is tested and analyzed using the developed model. Special attention is given to the residual stresses and time effects in curved members. Finally, the paper presents application of the layered timber construction to ribbed shell structures where results from experiments and computations using the developed linear elastic model are compared.

* Corresponding author.
E-mail address: mosalam@ce.berkeley.edu (K.M. Mosalam).

1359-8368/02/$ - see front matter © 2002 Published by Elsevier Science Ltd.
PII: S1359-8368(02)00020-3

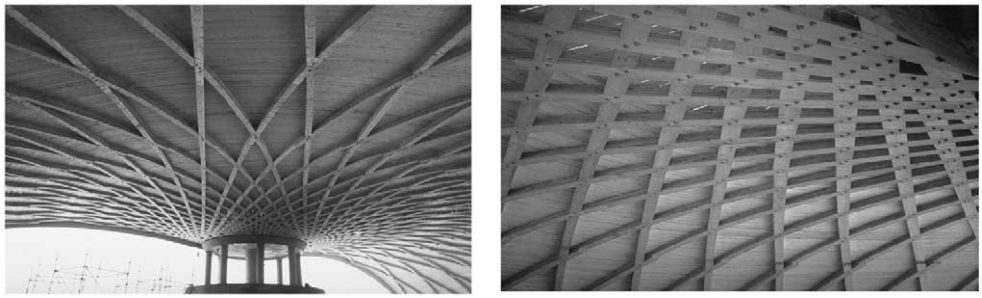

Fig. 1. Timber ribbed shell for an indoor pool in Saint-Quentin-en-Yvelines.

Summary and concluding remarks are presented at the end of the paper.

2. Computational model for layered timber beam

A computational model for calculating the deformation and stresses in layered composite beams is presented. This model handles beams consisting of multiple layers connected by semi-rigid joints such as those formed by glue, nails or dowels as shown in Fig. 2. This computational model is the basis for analyzing and designing timber beams in Appendix F of Ref. [6]. The model allows determination of internal force resultants, deflection of the beam, slip between the layers and shear and normal stresses at any point in the beam. The developed model represents an essential step for accurate and practical analytical and design procedure for timber ribbed shells. This model is simple enough to be easily implemented using available computer programs for structural analysis, such as the well-known program SAP2000 [2].

Several previous studies compared the outcome of the presented computational model to other methods using specific examples. Kreuzinger [9] compared the model results with the 'γ-procedure' presented in Ref. [6] and based on developments by Möhler [10] and Heimeshoff [8]. Gliniorz and Hübner [7] compared the results of the model with the exact mathematical solution based on the governing differential equation of beams. The conclusions from these comparisons are: (i) the developed multi-layer beam model is exact for situations with only two layers, (ii) the computational error for three up to seven layers is negligible, and (iii) in the case of more than seven layers.

2.1. Model description

The flexural rigidity of layer i in a multi-layer beam has a position independent part E_iI_i and a position dependent part $A_iz_{i,c}^2$ where E_i is the modulus of elasticity, I_i and A_i are the moment of inertia about the centrodial axis of layer i and its cross-sectional area, respectively, and $z_{i,c}$ is the distance between the center of layer i and the center of the multi-layer beam section. With this distinction, it is possible to split the beam into two independent beams, namely beam A and beam B, for the purpose of deformation and stress calculations. In formulating the properties of these two beams, the shear deformations at the joints between the layers have to be taken into account. In the current computational model, beam A is treated as shear-rigid while beam B accounts for the shear flexibility of the timber and the joints. It should be noted that beams A and B are constrained such that compatibility requirements are satisfied. This is satisfied by having the same elastic lines for both beams which is a possible option in the used computer program SAP2000 [2]. When the used program does not allow this option, one can utilize the rigid link model shown in Figs. 3 and 4.

As discussed before, the multi-layer beam is transformed into beams A and B connected with inextensible bars as shown in Fig. 3 with a schematic of the case of two layers. In this figure, the product of the timber shear modulus G and the cross-sectional area of beam B used for shear deformation A_z^{B} gives the equivalent shear stiffness S

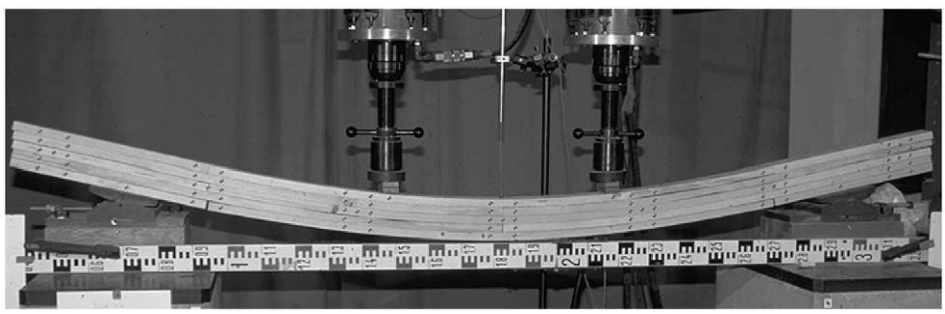

Fig. 2. Multi-layer beam under four point bending.

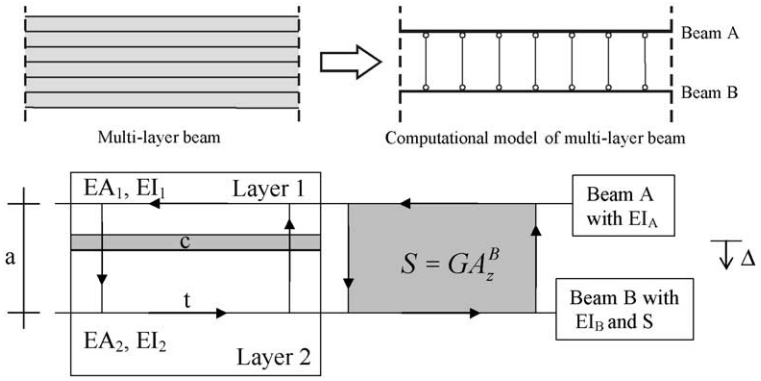

Fig. 3. The computational model of a multi-layer beam.

which represents the combined effect of the shear stiffness of the layers and the interface shear stiffness c. This modeling approach can be easily accommodated with many existing structural analysis programs. The tested beam in Fig. 2 is idealized with this model as shown in Fig. 4. In this computational model, beam A accounts for the sum of the individual stiffness properties of all layers forming the beam section and beam B represents the group effect of the layers according to their distances from the centroidal axis of the section. In addition, beam B accounts for the contribution of the elastic interfaces between the layers in terms of the stiffness of the joints. In the following discussion, the effect of torsion, i.e. drill degrees of freedom, is omitted for simplicity.

For the linear elastic solution of the problem, the properties of beam A include the flexural rigidity $EI_y^{\mathrm{A}} = \sum_{i=1}^{n} E_i b_i d_i^3/12$, the axial rigidity $EA_x^{\mathrm{A}} = \sum_{i=1}^{n} E_i b_i d_i$, and the cross-sectional area used for shear deformation $A_z^{\mathrm{A}} = A_x^{\mathrm{A}}/\kappa$ where E_i, b_i and d_i are, respectively, the modulus of elasticity, width and height of a rectangular layer number i for a beam with n layers and κ is a form factor taken as 1.2 for rectangular sections. On the other hand, the properties of beam B represents the combined effect of the layers within the multi-layer beam that depends on the beam geometry and the in-between layers joint stiffness. The flexural rigidity of beam B is $EI_y^{\mathrm{B}} = \sum_{i=1}^{n} E_i b_i d_i z_{i,c}^2$. Beam B is treated as having null axial load cross-sectional area, i.e. $A_x^{\mathrm{B}} = 0$. The effective shear load cross-sectional area of beam B is estimated according to $A_z^{\mathrm{B}} = S/G$ where S is the shear stiffness which is expressed by

$$S = a^2 b \Big/ \left(\sum_{1}^{n-1} \frac{1}{c_i} + \frac{d_1}{2G_1} + \sum_{i=2}^{n-1} \frac{d_i}{G_i} + \frac{d_n}{2G_n} \right), \tag{1}$$

where a is the distance between the centroids of the first and the nth layers and G_i and c_i are, respectively, the shear modulus of layer i and the joint stiffness between layers i and $i+1$. This joint stiffness can be estimated according to the design procedure in Appendix V of Ref. [6] for timber construction. Derivation of Eq. (1) is presented in Appendix A. It is to be noted that throughout the present study $G = G_1 = \cdots = G_n$ and $b = b_1 = \cdots = b_n$.

The shown example of a multi-layer beam in Fig. 4 has geometric vertical discontinuities of the timber planks. In this general situation, the idealized multi-layer beam into beams A and B should be allowed to have different properties along the axis of each beam. The computational model can easily accommodate these different zones of stiffness or different numbers or types of semi-rigid joints of the beam.

2.2. Computation of stresses

The stresses at any point in the multi-layer beam can be computed using the model described above. The internal forces in both beams A and B of this model are first evaluated when the model is analyzed under the given set of boundary conditions. These internal forces include the axial

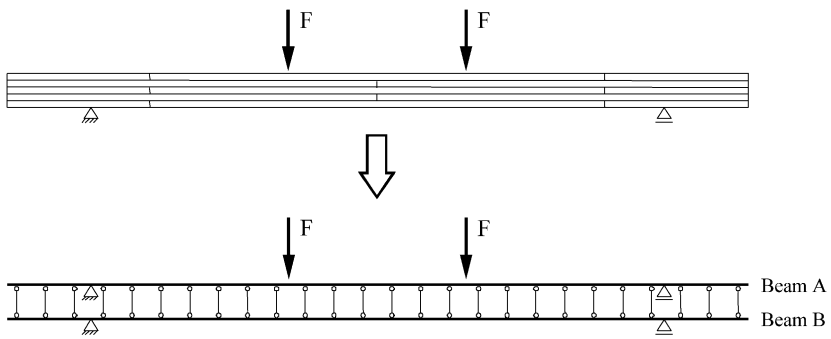

Fig. 4. The computational model of the beam shown in Fig. 2.

force N in beam A, the bending moments M_y^A and M_y^B in beams A and B, respectively, and the shear forces Q_z^A and Q_z^B in beams A and B, respectively. The constant normal stress in beam A due to N is obtained from $\sigma_x = N/A_x^A$. On the other hand, the varying normal stress due to M_y^A and M_y^B is obtained using

$$\sigma_{x,i}(z_i, z_{i,c}) = \sigma_{x,i}^A(z_i) + \sigma_{x,i}^B(z_{i,c}), \tag{2}$$

with $\sigma_{x,i}^A(z_i) = M_y^A z_i / I_y^A$, $-d_i/2 \le z_i \le d_i/2$ and $\sigma_{x,i}^B(z_{i,c}) = M_y^B z_{i,c}/I_y^B$. The shear stress due to Q_z^A and Q_z^B is obtained using

$$\tau_{xz,i}(z_i, z_{i,c}) = \tau_{xz,i}^A(z_i) + \tau_{xz,i}^B(z_i, z_{i,c}). \tag{3}$$

$$\tau_{xz,i}^A(z_i) = \left| Q_z^A \left(z_i^2/2 - d_i^2/8 \right) / I_y^A \right|. \tag{4}$$

$$\tau_{xz,i}^B(z_i, z_{i,c}) = \left| Q_z^B z_{i,c}(z_i + d_i/2)/I_y^B \right| + \tau_{xz,i-1}(-d_{i-1}/2, z_{i-1,c}). \tag{5}$$

2.3. Computation of deformations

The shear deformation of layer i, $u_i(z_{i,c})$ as shown in Fig. 5 is decomposed into joint slip $u_{F,i} = \tau_{xz,i}/c_i$ and the sum of shear deformations due to transverse forces in beams A and B, $u_{\gamma,i}(z_{i,c}) = u_{\gamma,i}^A + u_{\gamma,i}^B(z_{i,c})$, i.e.

$$u_i(z_{i,c}) = u_{F,i} + u_{\gamma,i}(z_{i,c}) = u_{F,i} + u_{\gamma,i}^A + u_{\gamma,i}^B(z_{i,c}). \tag{6}$$

The shear deformations depend on the angular changes, refer to Fig. 5, such that $u_{\gamma,i}^A = \gamma_i^A d_i$ and $u_{\gamma,i}^B(z_{i,c}) = \gamma_i^B(z_{i,c}) d_i$. These angular changes are obtained from the corresponding shear stresses, such that $\gamma_i^A = 2\tau_{xz,i}^A(0)/3G_i$ and $\gamma_i^B(z_{i,c}) = \tau_{xz,i}^B(0, z_{i,c})/G_i$.

3. Application of a layered timber beam

This section presents an application of the previously discussed computational model. This application is for the five-layer timber beam subjected to four point bending test shown in Figs. 2 and 4. All timber planks, with modulus of elasticity $E_x = 14\,700\ \mathrm{N/mm^2}$ and shear modulus $G = 880\ \mathrm{N/mm^2}$, have the dimensions $d_i = 27$ mm and $b_i = 78$ mm and are connected by semi-rigid joints in the form of corrugated nails with two different diameter/length ratios of 2.8/50 and 2.8/40 mm. The planks are staggered as shown in Fig. 6 where three basic regions can be identified. In region A, all five planks are continuous leading to homogeneous sections. In regions B and C, two and three of the five planks are discontinuous, respectively. This decrease in the cross-section stiffness is considered in the current beam application. The choice of this geometrical layout (with splices of the layers) of the timber planks is made to simulate a generic element in a larger framework of layered timber structure such as timber ribbed shells as discussed in Section 5. The nail schemes used for this beam are shown in Fig. 7.

3.1. Determination of stiffness of the joints between timber layers

The stiffness of the joint between the timber layers is estimated according to the design recommendations of Appendix V of Ref. [6] for timber construction. In the present application, the timber density ρ_w is assumed to be $420\ \mathrm{kg/m^3}$. The dowel diameter for the mechanical fasteners d_d is taken as 2.8 mm. Therefore, the joint stiffness per nail, defined as the shear force in one nail per unit sliding along the joint surface, $K_d = \rho_w^{1.5} d_d/20$ is estimated as 1205 N/mm. Each joint associated with a tributary area A_J equals the product of the width of the beam taken as 78 mm and the length along the beam axis taken as 80 mm, i.e. $A_J = 6240\ \mathrm{mm^2}$. The considered beam consists of five timber planks with four joints having the number of dowels given by $\{nd\} = \{1\ 2\ 2\ 2\}$ within A_J. Accordingly, the joint stiffness smeared over the interface area $c_i = K_d n d_i / A_J$ is given by $\{c\} = \{0.193\ 0.386\ 0.386\ 0.386\}\ \mathrm{N/mm^3}$. The theoretical joint stiffness in terms of K_d is applicable for small deformations as intended in Ref. [6]. A comparison between this theoretical value and the measured response for the two different joints $i = 1$ ($nd_i = 1$) and $i = 2$, 3, and 4 ($nd_i = 2$) is shown in Fig. 8.

3.2. Finite element analysis and comparison with experiment

To validate the proposed computational model of layered timber beams, finite element analysis (FEA) using the

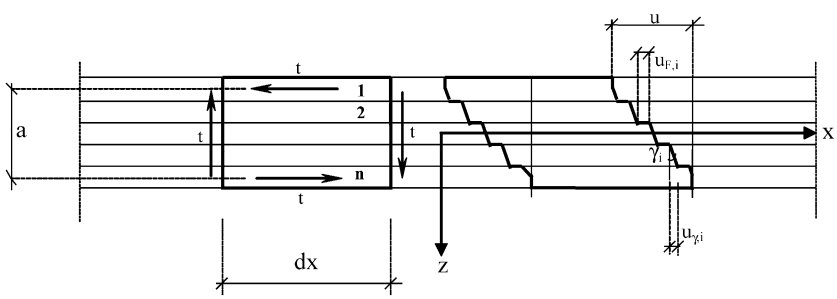

Fig. 5. Constant shear flow deformation of an infinitesimal element of a multi-layer beam.

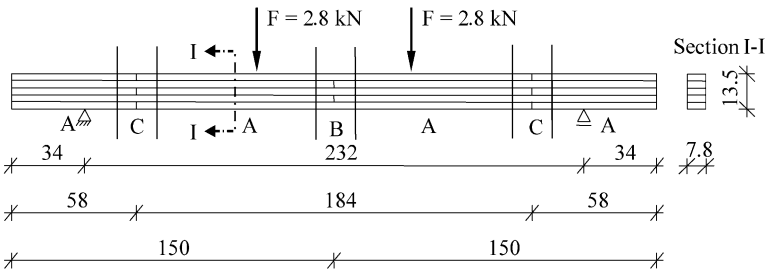

Fig. 6. Dimensions and regions of the test multi-layer timber beam (all dim. in cm).

program DIANA7.2 [3] is conducted. In this analysis, each plank is discretized using four node plane stress elements with orthotropic material properties ($E_x = 14\,700\ \mathrm{N/mm^2}$, $E_z = 1180\ \mathrm{N/mm^2}$, $G_{xz} = 880\ \mathrm{N/mm^2}$, and $\nu_{xz} = 0.15$). The elastic moduli are experimentally determined using ultra-sonic Sylvatest™ machine. As for Poisson's ratio and the shear modulus, common values are used. The vertical geometrical discontinuities between planks are accounted for in the finite element mesh. The interfaces between the different planks are modeled using four node zero-thickness line interface elements [11] with nonlinear properties in the tangential direction as shown in Fig. 8. In the normal direction of the interface, very large stiffness is considered for the compression mode to prevent penetration of planks while much smaller constant stiffness value is considered in the tension mode representing the limited pull out resistance

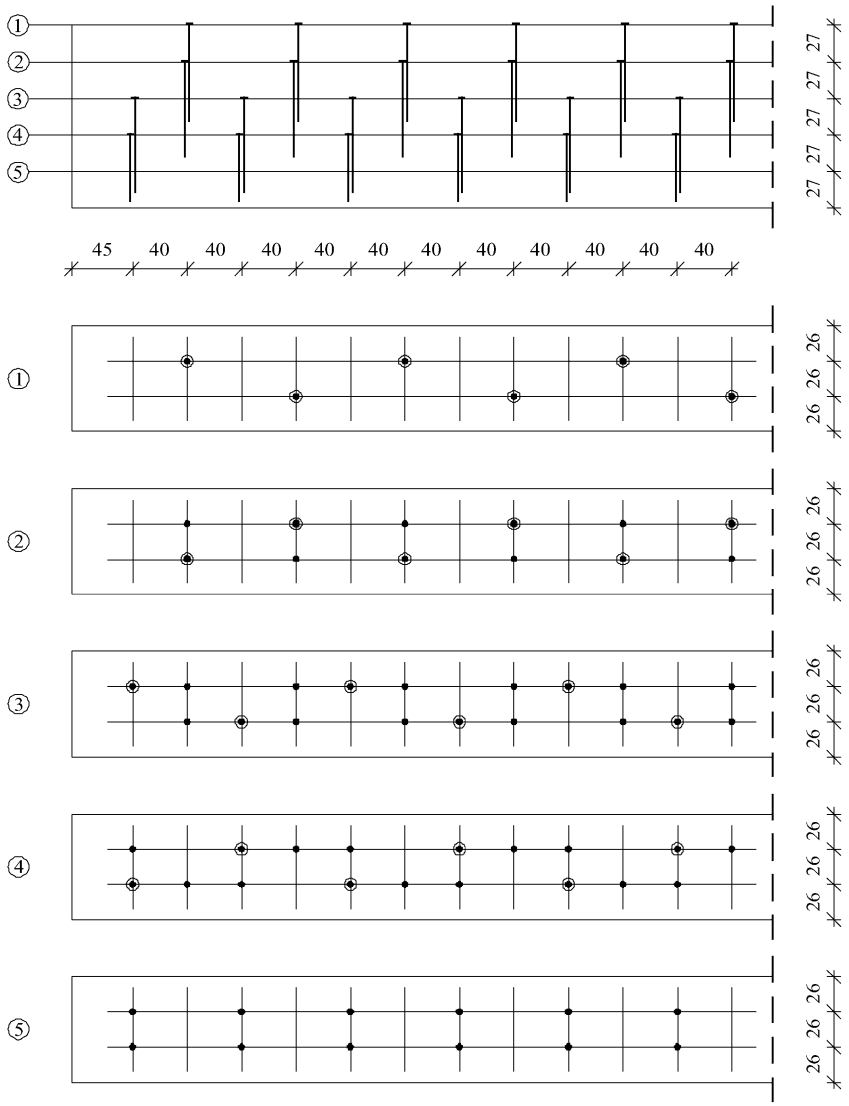

Fig. 7. Elevation and plans for the nail schemes (all dim. in mm).

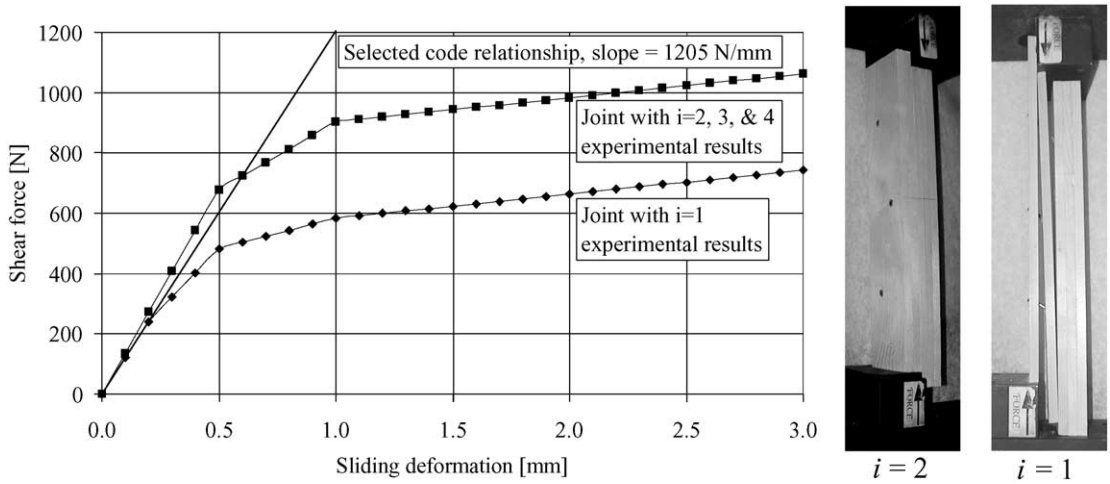

Fig. 8. Response in the tangential direction of different timber joints.

of nails. The nail pull out properties are based on the model given in Ref. [4] where for the considered geometrical and material properties, this normal stiffness is estimated to be 875 N/mm, i.e. approximately 70% of the code shear stiffness is shown in Fig. 8.

The nonlinear solution using the FEA is conducted using incremental-iterative procedure to trace the nonlinear response. For each increment, equilibrium iterations are performed based on Newton–Raphson method where the stiffness matrix is updated at each iteration. The iteration process stopped when the convergence criterion based on the energy norm $|E| = |_i\{\delta u\}^{\mathrm{T}}\{_{i+1}\{f_{\mathrm{int}}\} +_i \{f_{\mathrm{int}}\}\}/_0\{\Delta u\}^{\mathrm{T}}\{_1\{f_{\mathrm{int}}\} +_0 \{f_{\mathrm{int}}\}\}| \leq 10^{-5}$ was satisfied. In this norm, $\{\delta u\}$ and $\{\Delta u\}$ are vectors of iterative and total displacement increments, $\{f_{\mathrm{int}}\}$ is the internal force vector, superscript T indicates transpose, and left subscripts of the vectors indicate iteration number.

The experimentally determined load–deflection curve and portion of the deformed shape near a vertical discontinuity in the planks for the beam shown in Fig. 6 is compared with those obtained from the FEA in Fig. 9. The load–deflection results of the FEA include that based on nonlinear model for the interface between the planks and that based on linear model following the code relationship of Fig. 8 and for applied force $F = 2.8$ kN as shown in Fig. 6. From these comparisons, one concludes that the FEA

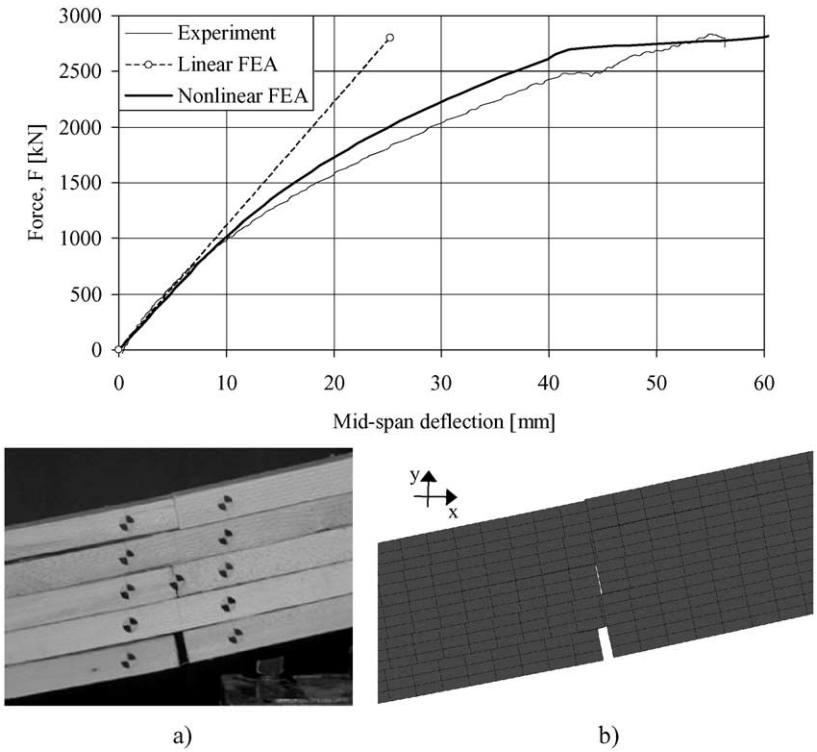

Fig. 9. Comparison between experimental and FEA deformed shapes at region C of Fig. 6. (a) Experimental deformed shape and (b) FEA deformed shape.

Table 1
Section properties for the multi-region layered timber beam shown in Fig. 6

Region	n	A_x^A (cm^2)	A_z^A (cm^2)	I_y^A (cm^4)	I_y^B (cm^4)
A	5	105.30	87.80	64.00	1535.30
B	3	63.18	52.65	38.40	1228.22
C	2	42.12	35.10	25.60	307.05

model captured the nonlinear response of the beam with reasonable accuracy.

3.3. Determination of section properties

The section properties of the multi-layer timber beam are determined based on the planks layout shown in Fig. 6. For the stresses due to axial forces, the cross-sectional area is the superposition of the planks that are continuous in the corresponding region. This is the case because the vertical discontinuities between the planks, where stiffness jumps exist, do not close under loading. This is accounted for in the reduced flexural stiffness regions B and C (Fig. 6) where the length of each of these regions is taken as the distance between the section of vertical discontinuities of planks to the first mechanical fastener on both sides of the section, i.e. a total length of 80 mm (refer to Fig. 7). Table 1 presents the section properties for the analyzed beam in Fig. 6 for the different regions comprising the beam.

The common section properties to all regions of the beam are based on the distance a defined in Fig. 5 as 10.8 cm. Accordingly, the shear stiffness S, Eq. (1), is estimated as 69.6 kN. Subsequently, the cross-sectional areas for beam B are estimated as $A_x^B = 0.0$ and $A_z^B = 0.79$ cm^2.

3.4. Results and comparisons

The beam shown in Fig. 6 is analyzed using the proposed linear computational model of layered timber beams. This application is performed using the structural analysis program SAP2000 [2]. The maximum deflections at mid-span Δ_{max} from SAP2000 and based on linear FEA using DIANA7.2 [3] with $F = 2.8$ kN are 26.0 and 25.3 mm, respectively. Obviously, good agreement is obtained between the computational model and finite element solution.

Comparisons between the proposed computational model (beams A and B) and the FEA using linear elastic solution for the normal stress distributions at the identified sections A–A and B–B are shown in Fig. 10. The comparison in Fig. 10 is excellent for the normal stresses not only at section A–A and but also at section B–B which has geometric discontinuity.

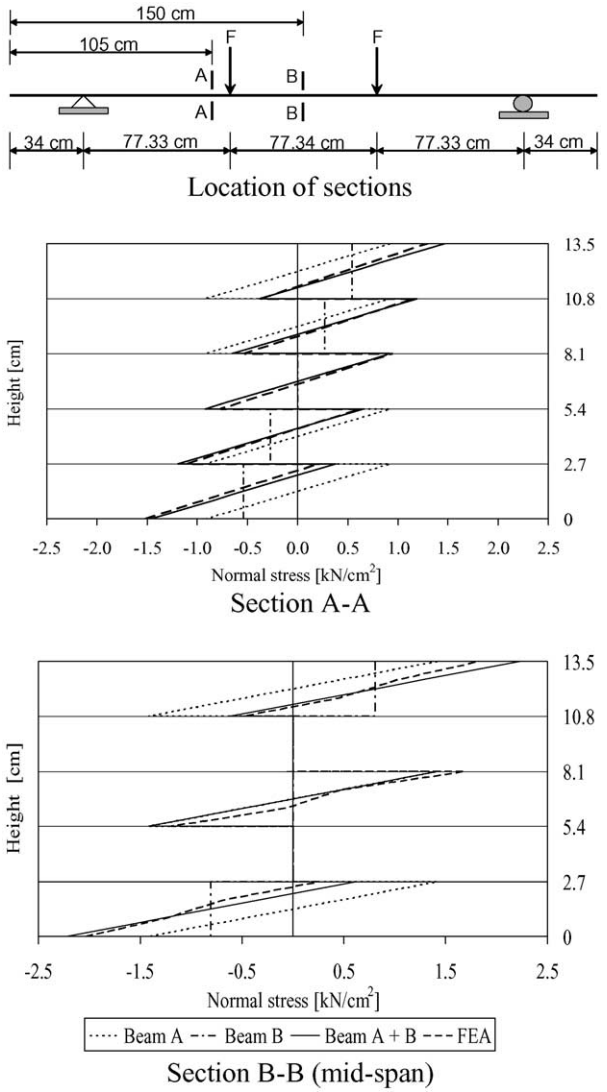

Fig. 10. Computed normal stress distributions at sections A–A and B–B of test beam.

4. Extension to layered curved timber beam

The model for layered timber beam is extended to account for curved members for further application to timber ribbed shells. The main focus of this extension is the treatment of residual stresses during construction due to the curved geometry of the beam. Although this extension should be approached using curved (not straight) beam theory, this fact is ignored here since in layered curved timber beams, the construction effects has greater influence than the assumptions in applying straight beam theory for curved members. Moreover, from a practical point of view, the layered curved timber beams are usually of large spans indicating that the error involved in the use of straight beam theory may be negligibly small. This is further justified by the reasonable match with the experimental findings for a tested arch with relatively small radius, as shown in Section 4.3.

4.1. Residual stress within curved beams

It is known that the bending radius of a curved timber

plank forming one layer of a multi-layer curved beam which may be used as a rib of a timber ribbed shell, should be approximately greater than 200 times the plank thickness [6]. This is the case to limit the residual stress within the timber-ribbed shell by limiting the curvature and distortion of its elements. Normally, the radius of shell structures is so large that such residual stress of the members can be neglected. Although this is the case on a global level, a complex form of the shell may have local small radii of the ribs mandating proper treatment of the residual stresses due to construction.

Layered curved timber beams are assembled using a prefabricated template as shown in Fig. 11. The increase in the bending stresses by the curvature of the beam is inversely proportional to the beam radius r and increases from outside to inside where r decreases by the beam cross-sectional height. In the following computational model, this variation is disregarded where r is taken up to the beam centroidal axis.

A multi-layer curved beam can be fabricated by fixing the ends of arched planks as shown in the right part of Fig. 12(a) where a fixed end moment is generated for each layer i, $M_{\mathrm{F}i} = EI_i/r$. Accordingly, the total fixed end moment for a multi-layer curved beam formed by disjointed n layers become

$$M_{\mathrm{F}} = \sum_{i=1}^{n} M_{\mathrm{F}i} = nEI_i/r = EI_y^{\mathrm{A}}/r. \tag{7}$$

The constant bending moment in Eq. (7) implies no shear stresses between the layers. Accordingly, providing mechanical fasteners or glue between the layers, as shown in the left part of Fig. 12(a), will not affect the internal forces. If the fixed end moment M_{F} is released after mechanical fasteners are provided, shear stresses are imposed at the joints. In addition, with the release of all external boundary conditions, the curved beam deforms as shown in Fig. 12(b) where the curvature $1/r$ is reduced to $1/r_3$ by $M_{\mathrm{F}}/(EI_y^{\mathrm{A}} + EI_y^{\mathrm{B}})$, i.e.

$$\frac{1}{r_3} = \frac{1}{r}\left(1 - \frac{EI_y^{\mathrm{A}}}{EI_y^{\mathrm{A}} + EI_y^{\mathrm{B}}}\right) = \frac{1}{r}\left(\frac{EI_y^{\mathrm{B}}}{EI_y^{\mathrm{A}} + EI_y^{\mathrm{B}}}\right). \tag{8}$$

Finally, the maximum residual stresses (at extreme fibers) can be calculated such that,

$$\sigma_{x,\max}^{\mathrm{resid}} = M_{\mathrm{F}}/W_y = M_{\mathrm{F}}/\sum_{i=1}^{n} W_{yi} = M_{\mathrm{F}i}/W_{yi}, \tag{9}$$

where $W_{yi} = bd_i^2/6$ is the section modulus for layer i in an n-layered beam. It should be noted that this residual stress is solely due to the circular construction of the arch.

After the construction of a layered curved timber beam, the beam is supported as shown in Fig. 13. In this figure, a general case of circular arch with pin supports is shown where a constant bending moment M_{F} due to the construction process is shown uniformly distributed on a partial length of the arch. Applying the principal of virtual work, one can determine the reactions, $H_{\mathrm{A}} = H_{\mathrm{D}}$ and $V_{\mathrm{A}} = V_{\mathrm{D}}$ using the following equations,

$$r\int_{\zeta_1}^{\zeta_4}(H_{\mathrm{D}}\sin\phi - V_{\mathrm{D}}(1-\cos\phi))\sin\phi\,\mathrm{d}\phi + M_{\mathrm{F}}\int_{\zeta_2}^{\zeta_3} \times \sin\phi\,\mathrm{d}\phi = 0. \tag{10}$$

$$r\int_{\zeta_1}^{\zeta_4}(H_{\mathrm{D}}\sin\phi - V_{\mathrm{D}}(1-\cos\phi))(1-\cos\phi)\mathrm{d}\phi + M_{\mathrm{F}}\int_{\zeta_2}^{\zeta_3} \times (1-\cos\phi)\mathrm{d}\phi = 0, \tag{11}$$

where all notations are defined in Fig. 13. Knowing the angles ζ_1, ζ_2, ζ_3, and ζ_4, the radius r and using Eqs. (7), (10) and (11), one obtains the reactions H_{D} and V_{D}. The special case of constant bending moment distributed over the whole length of a half circle correspond to $H_{\mathrm{A}} = H_{\mathrm{D}} = 4\pi M_{\mathrm{F}}/r(3\pi^2 - 16)$ and $V_{\mathrm{A}} = V_{\mathrm{D}} = 2(\pi^2 - 8)M_{\mathrm{F}}/r(3\pi^2 - 16)$.

During the fabrication process of the tested multi-layer curved timber beam of Fig. 11, the planks are shaped into an arch using fixed timber blocks and fasteners connecting the arch to the blocks as shown in Fig. 11. At this stage, the joints between the planks are not activated, i.e. there is no sliding along the interfaces. Prior to placing the joined multi-layer curved beam on the supports for testing under in-plane loading, these fasteners are removed starting from the arch crown and proceeding towards the ends. In this process, the radius of the arch at the crown increases with the removal of fasteners, as shown in Fig. 14(a). The last two fasteners at the arch ends during fabrication exert the

Fig. 11. Fabrication of multi-layer curved timber beam.

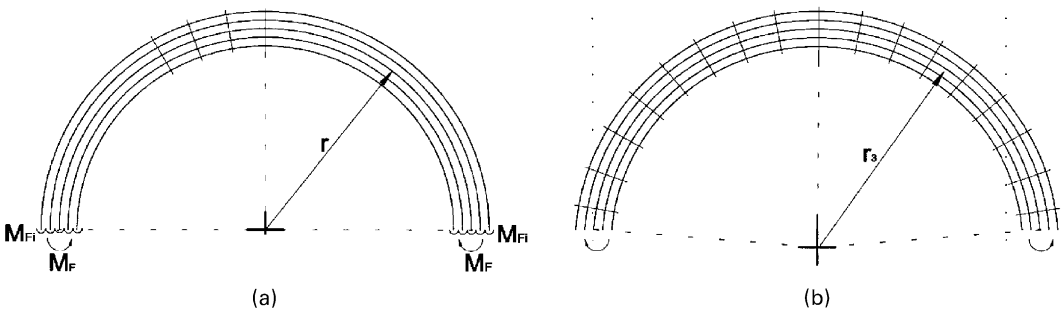

Fig. 12. Boundary conditions and deformation of layered curved beam during construction.

self-equilibrating forces H_F on the arch as shown in Fig. 14(a). As discussed previously, the deformed shape of the arch during fabrication calls for constant residual bending moment as shown in Fig. 14(b) which can be modeled using the end couple formed by the two equal and opposite forces H_F and Z with a distance l_1 in between, Fig. 14(b).

In the computational model for determining the residual stresses, instead of the couple formed by the forces H_F and Z and the distance l_1, the same effect can be accomplished using vertical forces V_1 and V_2 with eccentricity e as shown in Fig. 15. These forces are applied to beam A only since beam B has null axial force cross-sectional area. This choice of forces, analogues to internal pre-stressing, is viewed to be simpler in design where one deals with statically determinate structural systems. In this case, e can be arbitrarily selected and the corresponding force is calculated from

$$V_1 = -V_2 = M_F/e = EI_y^A/er. \tag{12}$$

4.2. Time effect on residual stress within curved beams

The residual stress in timber structures decreases with time due to creep effect. During the design process of ribbed timber shells, engineers control the stresses during construction and under different loading conditions. The time-varying residual stresses due to the construction procedure should be included with the stresses due to service loading. An in-depth study of this topic is out of the scope of the paper but the importance of creep effects requires attention

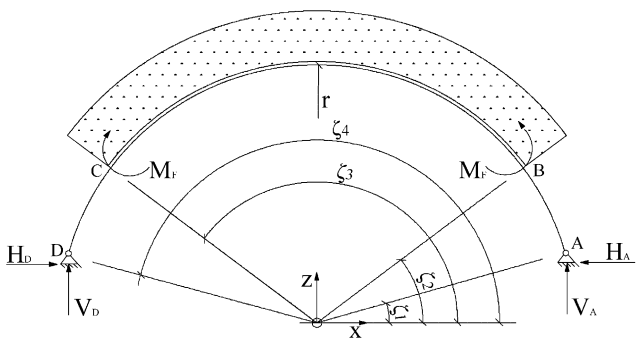

Fig. 13. Circular arch subjected to constant bending moment due to construction.

from the engineers when dealing with residual stresses due to construction. A design approach is to adopt a reduction coefficient C_t to account for the time effect on the residual stresses. This factor is a function of time and can be applied to reduce the force couple in Eq. (12). Different publications show creep functions, which were established accounting for the influence of time on the stress level under different conditions. In Ref. [6], a simple modification of Eq. (9) is suggested where $\sigma_{x,\max}^{\text{resid}} = C_t M_F / \sum_{i=1}^{n} W_{yi}$ with C_t is a time-dependent reduction coefficient which is given by $C_t = \exp(a(t))$ for timber structures with timber moisture content between 10 and 16%. For design, the most important cases are: (i) at construction, $a(0) = 0$, and (ii) at the end of live cycle, $a(\infty) = 0.6$.

4.3. Application

Figs. 16 and 17 show the geometry and boundary conditions of a multi-layer curved timber beam tested under asymmetric loading conditions. Plank dimensions and material properties were identical to those used in the layered beam test of Fig. 2. The test was conducted monotonically up to a load value $F = 4$ kN. During the experiment, photographs were taken and processed afterwards to determine the continuous deflected shape of the arch. At the indicated load level, good agreement between the experimentally and computationally determined deflected shapes is evident from Fig. 18. In this case, the effect of pre-stressing (Eq. (12)) of the arch was shown to be small due to the relatively large ratio of arch radius to plank thickness. In other cases, where high local curvatures exist such as in ribbed shell construction, the effect of pre-stressing to account for residual stresses is expected to be significant.

5. Experiment and analysis of timber ribbed shells

5.1. Background

One of the first timber shells is constructed at the beginning of the 20th century by the German civil engineer Zollinger [1]. In Zollinger's construction, all members of the shell have the same dimensions as shown in Fig. 19

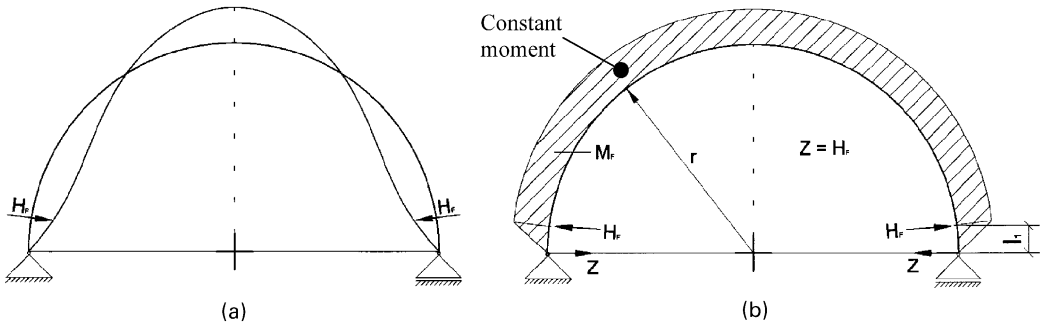

Fig. 14. Modeling effect of end fasteners on supported curved timber beam.

where two members are connected to the middle of another member. This connection point of the timber members is obtained using a nail or a dowel through all members meeting at that point. An advantage of this construction method is the possibility of pre-fabrication and fast assembly. The success of this method is dependent on the finishing accuracy of the timber members.

During the 1970s, several multi-section timber ribbed shells were constructed in Europe. Each member of the ribs is build up from pilled timber planks joined by nails or dowels. These ribs represent a curved floor grid which works together with a continuous curved floor made of thin boards to form high load bearing shell structure.

5.2. Fabrication of timber ribbed shells

There are two construction methods to fabricate timber ribbed shells. In the first method, simple pre-fabricated forms are laid flat on the construction site. In this case all timber planks are pilled flat and joined loosely by a dowel at the cross-point of the ribs. The form shape is maintained using temporary supports. Subsequently, the whole structure is lifted in the finished position using a fixed pillar crane (Fig. 20(a)). Once the structure is in the final position, all layers of the ribs are joined by screws or nails and the dowels tightened. In the second method, a soffit scaffolding (false-work) taking the form shape of the shell is constructed (Fig. 20(b)). The different positions of the ribs are labeled on the false-work where the planks are first laid and fixed temporarily. Filler blocks are cut and fixed on the first plank layer at the cross-points by dowels. This is repeated for other layers where the bolts at the cross-points of the ribs serve as mounting devices for the subsequent layers. Finally, before the false-work is removed, the covering boards are joined by nails or dowels on the ribs.

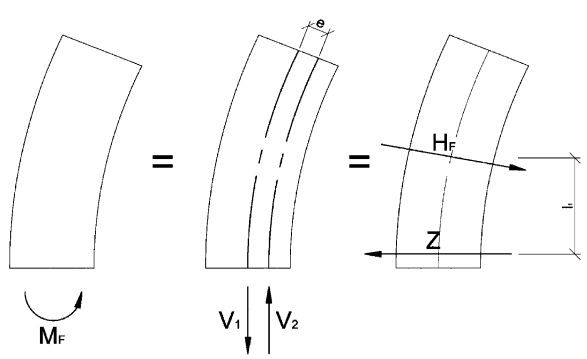

Fig. 15. Possibilities to induce a constant bending moment distribution in the curved beam.

5.3. Details of experimental cross-ribs

To demonstrate the performance of timber ribbed shells and to validate the developed computational model of layered timber beams and arches, an experimental object of cross-ribs is tested as shown in Fig. 21(a). In this case, all layers of the ribs are connected at the cross-points using 8 mm diameter machine bolts with turning moment of 15 kN m (Fig. 21(c)). This turning moment was checked just before load application. Between the cross-points, timber layers are joined using 3.5 mm diameter screws (Fig. 21(b) and (d)).

The relatively small radius of the curved timber planks (Fig. 21(a)) results in high residual stresses, as discussed in Section 5.2. To prevent splitting of the layers during construction, these layers were pilot-drilled using 1.5 mm diameter holes.

The cross-ribs joined the foundation through a 6 mm thick Neopren pad as shown in Fig. 21(e). This foundation consists of fixed plywood plates. The restraining horizontal force of each curved rib, i.e. reactions H_A and H_D in Fig. 16 are resisted by 6 mm steel 37 rods as shown in Fig. 21(a) and (e). Each of these rods was conservatively designed to carry

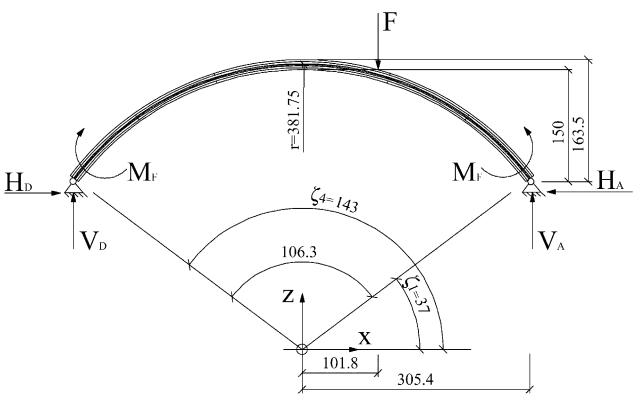

Fig. 16. Geometry and boundary conditions of the tested arch (dim. in cm).

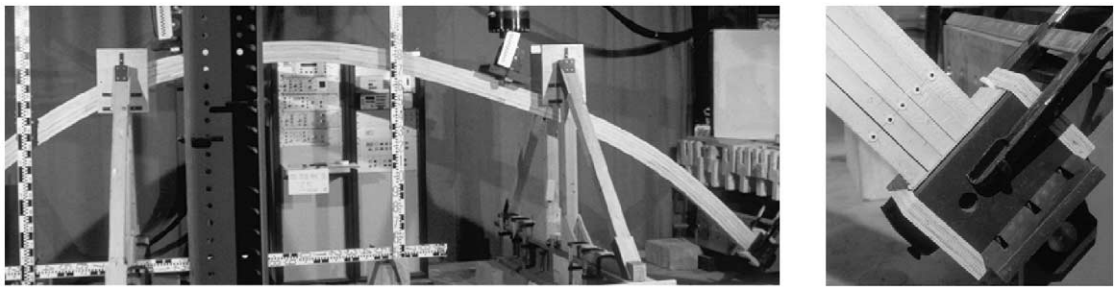

Fig. 17. Loading of the tested arch with close up at the supports.

twice the force of each rib ($H_A = H_D = 1.225$ kN) accounting for the fact that two ribs intersect at each support point.

5.4. Shape and geometry of the experimental cross-ribs

For the computational modeling and design of ribbed shells, exact description of the shell geometry is necessary. Each cross-rib is mathematically analogous to a helical line on a cylindrical surface [5]. Following the coordinates of a helical line shown in Fig. 22(a), one defines $x = r\cos\varphi$, $y = r\sin\varphi$, and $z = c\varphi$. The geometrical data of the cross-ribs of Fig. 21(a) are the radius $r = 1250$ mm and the helix pitch $2\pi c = 2000$ mm. The length s of one timber plank between the limits $\varphi = 0$ and $\varphi = \pi$ is expressed as $s = \pi\sqrt{r^2 + c^2} = 4052$ mm. The helix is characterized by central angle $0 \le \varphi \le \pi$, sweep $\kappa = 1/a = r/(r^2 + c^2) = 1/1331\ \text{mm}^{-1}$, and twisting $\vartheta = c/(r^2 + c^2) = 1/5227\ \text{mm}^{-1}$.

5.5. Computations of timber ribbed shells

The timber ribbed shell can be analyzed using three-dimensional structural analysis software such as SAP2000 [2], refer to Fig. 22(b). The ribs are represented by curved beams intersecting at the cross-points. Between these points, other nodal points are introduced for accurate representation of the curved geometry. Every rib of the test cross-ribs in Fig. 22(a) is divided into 144 elements. At the cross-points of the ribs, two nodal points with the same coordinates are used; one for each of the two intersecting ribs. At these double nodes, all degrees of translational and rotational degrees of freedom are constrained between the two nodes except the rotations about the two local rib axes normal to the tangents of the two ribs at each cross-point.

The computational model of the timber ribbed shell is based on substituting each multi-layer timber rib with two beams A and B connected by inextensible bars as discussed for the case of straight multi-layer timber beams, Fig. 3. Since the ribs are curved in space, transverse loading produces bi-directional flexural stresses in the corresponding curved beams leading to a more complex state of stress than that of straight beams.

For each multi-layer curved beam, the moment of inertia I_z about the local z-axis is split in beams A and B in proportion to the inertias about the local y-axis, i.e.

$$I_z^A = I_z I_y^A / \left(I_y^A + I_y^B\right) \text{ and } I_z^B = I_z I_y^B / \left(I_y^A + I_y^B\right). \tag{13}$$

It is noted that the curved beam when deflected in the local y-direction is assumed to behave as a homogenous beam without the influence of the interfaces between the layers. In addition to the bi-directional bending moments of the curved beam, torsional moments also exist. For this purpose, the elastic estimate of the section torsional rigidity GI_T of n semi-rigidly connected timber planks is established as a range of values between that of loosely stacked planks and rigidly connected ones, i.e.

$$Gnbd^3/3 < GI_T < Gb(nd)^3/3, \tag{14}$$

where each plank has the cross-sectional width b and height

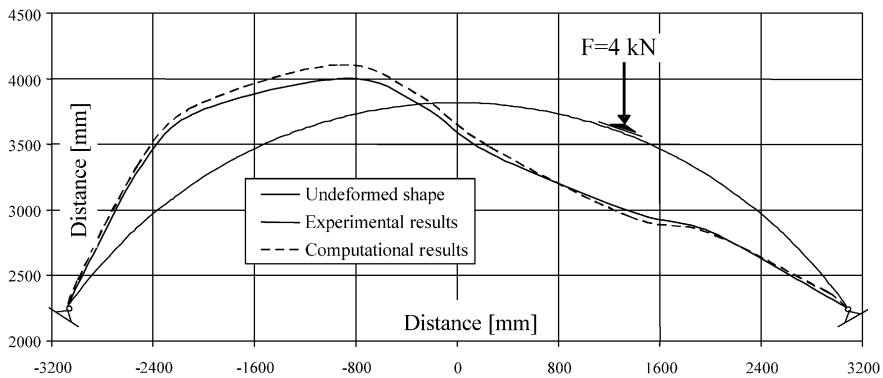

Fig. 18. Comparison between experimental and computational deflected shapes (amplification factor = 5) of the tested timber arch.

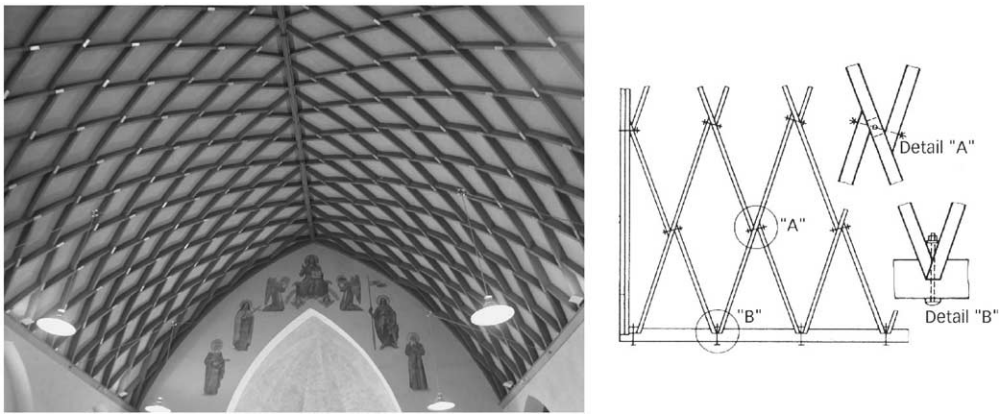

Fig. 19. Zollinger's timber shell construction and details [1].

d with $b \gg d$. It is to be noted that, for typical dimensions of the beams, the influence of the torsional stiffness of the ribs on the computational results is small. Accordingly and for simplicity, the torsional rigidity is estimated based on the assumption of rigidly connected planks. Moreover, the split of the torsional rigidity between beams A and B follows the same rules as that of I_z (Eq. (13)).

5.6. Application

The experimental object shown in Fig. 21(a) represents a cylindrical shell without the covering boards where all ribs are pin supported. Each cross-rib consisted of five planks with dimension $b = 70$ mm and $d = 8$ mm. The shell was tested under load control by a single load F at mid-span as shown in Figs. 21(a), 22(b) and 23. The loading of the shell was conducted mainly under monotonically increasing load control for the applied force F. This loading was preceded by two cycles up to $F = 1.2$ kN where the shell remained elastic with the corresponding maximum deflection $\Delta_{max} = 26$ mm. The results in the form of deflected shapes are presented at two load levels for $F = 1.2$ and 1.76 kN. During testing, applied load was recorded in addition to the deformation of all rib-nodes in the marked area (representing one quadrant of the shell) of Fig. 23 using three Theodolites with an accuracy of 0.05 mm. Moreover, the deformation between the layers at two cross-sections of the curved rib marked A in Fig. 23 were measured using optical glass-fiber sensors. Rib A is used to represent the deformation results for both the experimental and the computational studies.

Using the recordings of the three Theodolites, the deformation of the ribbed shell cross-points are calculated. These deformations are shown in Fig. 24 for the identified rib A in Fig. 23. As shown in Fig. 23, only measurements on half of rib A were taken making use of the expected symmetric response. This symmetry property was utilized in generating the results of Fig. 24 for the two indicated load levels. For clarity of presentation, the results in Fig. 24 are given in two separate projections of the rib in xy and yz planes according to the global axes shown in Fig. 23. From the results shown in Fig. 24, the calculated deformations of the shell structure reasonably agreed with the test results with maximum error 12.4% at the point of load application

(a)

(b)

Fig. 20. Construction methods of timber ribbed shells. (a) First method and (b) Second method.

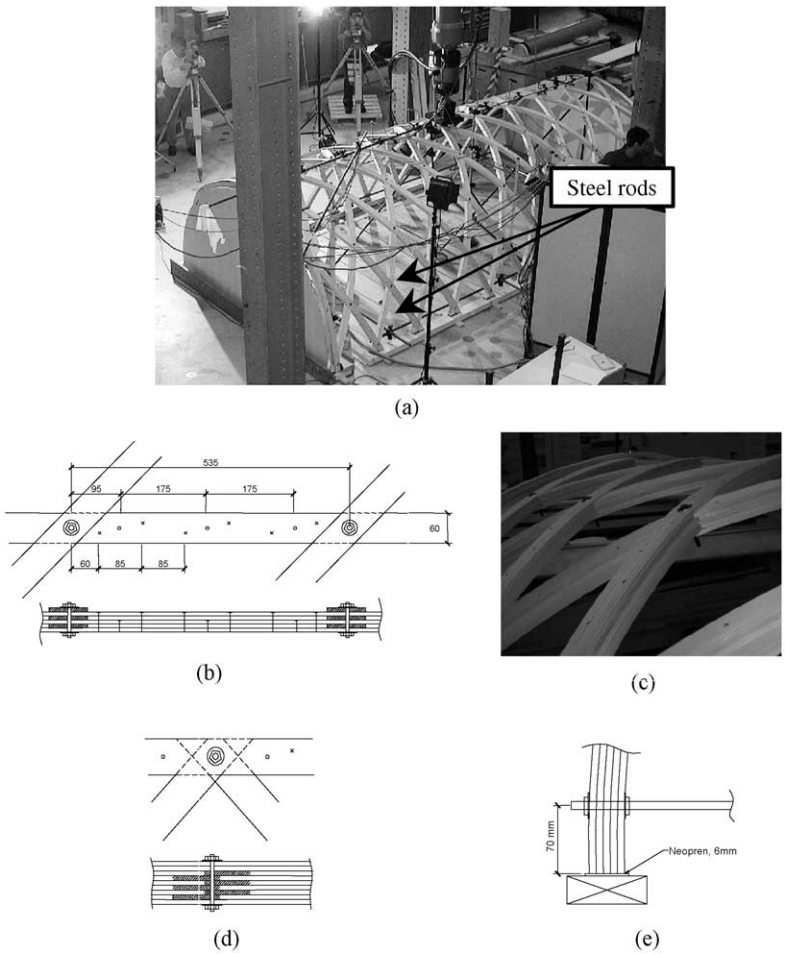

Fig. 21. Test specimen and details of timber cross-ribs. (a) Experimental object of cross-ribs, (b) Dowling scheme and cross-points [dim. in mm], (c) Cross-points of ribs, (d) Cross-point at edge, and (e) Detail of support.

for load level $F = 1.76$ kN. It is to be noted that the experimental results were underestimated near the point of load application and overestimated near the supports of the ribs. This is attributed to locally nonlinear response (sliding) of the joints between the planks of the ribs near regions of maximum deflection. This was identified from the in-between layer deformations (maximum of approximately 0.08 mm) recorded using optical glass-fibers with an accuracy of 2 μm. However, near the supports the actual response of the joints was linear. As the computational model utilizes an average linear representation of the joint stiffness (refer to Fig. 8), the discrepancy between the experimental and computational results can be explained.

6. Concluding remarks

The presented modeling technique of multi-layer

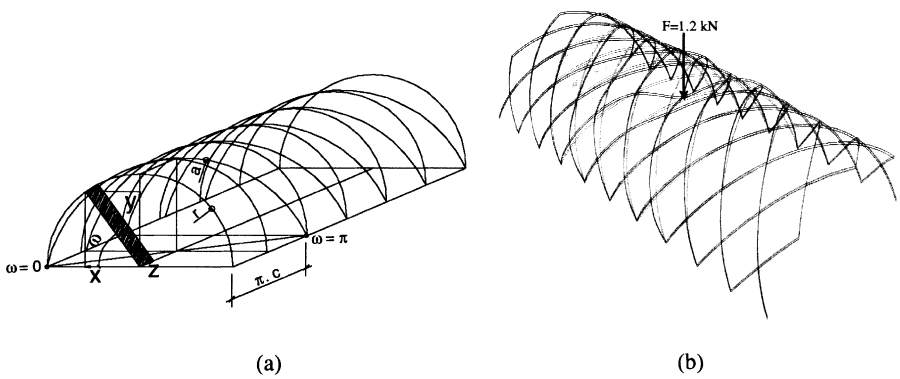

Fig. 22. Modeling of timber ribbed shells. (a) Shape and geometry of spiral-like planks and (b) Computational model of timber cross-ribs.

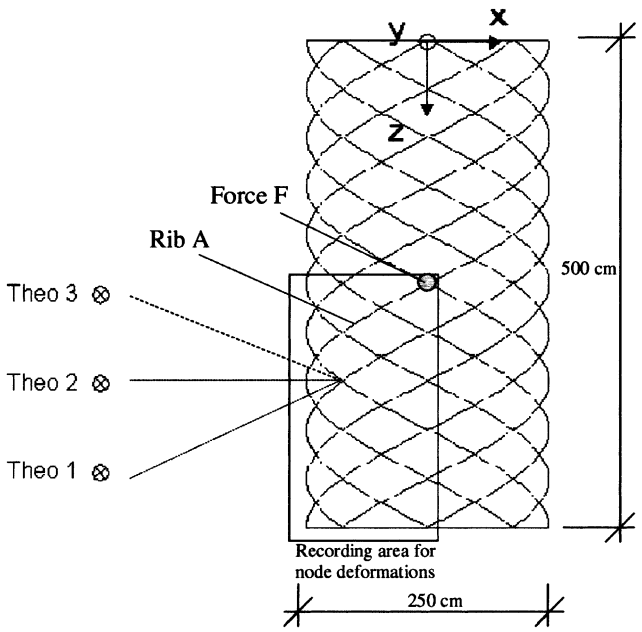

Fig. 23. Loading and deformation measurements on a plan view of the test cross-ribs.

structural members and systems is shown to be a valid practical approach for estimating the linear response of layered structures. This was clearly demonstrated using applications of timber beams, arches, and ribbed shells. Static experiments and detailed linear and nonlinear finite element analyses were used to demonstrate the validity of the modeling approach of multi-layered timber beams. The model emphasizes the possible sliding between layers due to the finite stiffness of the connections. This modeling method is general and can be used for many applications of layered structures. Moreover, commonly used structural analysis programs can be used to implement such models of layered structures. As a future extension of the developed model is the consideration of layered beam buckling and nonlinear effects. This is particularly important in applying the model to slender elements such as those commonly used in shell construction.

Extensions of the modeling of layered beams to include curved members and three-dimensional geometry were shown through the applications of multi-layered timber arches and layered cross-ribbed shell structures. For arch structures, special treatments of the residual stresses due to construction method and the time-dependent effects of timber were presented. The residual stresses due to the curvature of the member were treated using the concept of pre-stressing which is shown to be practical and easy to implement. The experimental results of deformation matched very well the computational predictions for the case of the multi-layered timber arch.

Several shells of the past were constructed according to engineering intuition without computational logic or model. In this study, the three-dimensional experimental object of cross-ribbed timber shell structure gave deformation results in a reasonable agreement with the computational prediction where the largest error was less than 13%. Accordingly, one concludes that a systematic modeling approach of timber shells is now possible. As a final note, application of the developed model for timber ribbed shell including the covering boards will be pursued in a future study. In this case, identifying accurate yet practical approach to model these boards and their connections to the cross-ribs will be a challenging task.

Acknowledgments

The financial support of the Swiss National Foundation is gratefully acknowledged. The experimental work of this

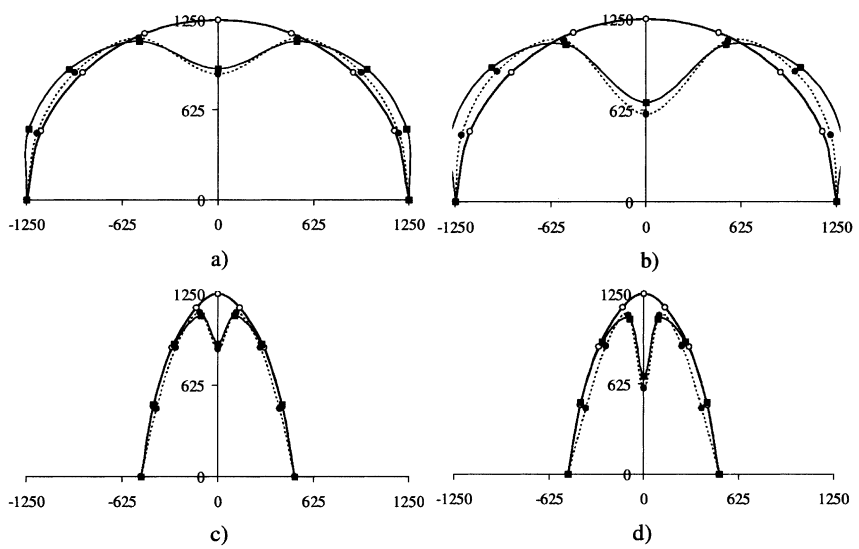

Fig. 24. Deformation results (amplification factor = 25) of the test cross-ribs. (a) *xy* plane at $F = 1.2$ kN, (b) *xy* plane at $F = 1.76$ kN, (c) *yz* plane at $F = 1.2$ kN, and (d) *yz* plane at $F = 1.76$ kN. –○– represents Original rib A, ···•··· represents Measured, and –■– represents Computed.

study was conducted at the Swiss Federal Institute of Technology, Lausanne. The research assistance of Maria Stolper, Claudio Pirazzi, and Lorenz Hübner and the technical assistance of Eric Tonicello and Francois Perrin, the laboratory manager, are appreciated. The computational work of this study was conducted at the University of California, Berkeley (UCB). The computational programs were provided through financial support from the College of Engineering at UCB and from donations of Computers and Structures, Inc. at Berkeley, CA.

Appendix A. Derivation of Eq. (1)

Estimation of S using Eq. (1) is based on an expression for the deformation u of a multi-layer beam subjected to shear flow t. This shear flow is applied between the centers of the outermost layers having distance a in between, as shown in Fig. 5 for an infinitesimal element along the beam axis. This shear flow can be converted to a constant value for the whole cross-section $t\kappa$ using the form factor κ. Accordingly, for layer i, the shear force is $t\kappa d_i$ and the shear strain γ_i is constant with $\mathrm{d}u = \gamma_i\,\mathrm{d}z$. The corresponding deformation $u_{\gamma,i}$ is obtained by

$$u_{\gamma,i} = \gamma_i \int_0^{d_i} \mathrm{d}z = (t\kappa d_i)/(b_i d_i G_i) \int_0^{d_i} \mathrm{d}z = \frac{t\kappa d_i}{b_i G_i}.$$

For the lower $i = 1$ and the upper $i = n$ layers, the deformations are given by

$$u_{\gamma,1} = (t\kappa d_1)/(b_1 d_1 G_1) \int_{d_1/2}^{d_1} \mathrm{d}z = \frac{t\kappa d_1}{2b_1 G_1},$$

and

$$u_{\gamma,n} = (t\kappa d_n)/(b_n d_n G_n) \int_0^{d_n/2} \mathrm{d}z = \frac{t\kappa d_n}{2b_n G_n},$$

respectively. By definition of the joint stiffness c_i for joint i between layers i and $i+1$, the additional deformation at this joint is given by $u_{\mathrm{F},i} = t\kappa/b_i c_i$.

From the above, the total displacement of the multi-layer section is given by

$$u = t\kappa\left(\sum_1^{n-1} \frac{1}{b_i c_i} + \frac{d_1}{2b_1 G_1} + \sum_{i=2}^{n-1} \frac{d_i}{b_i G_i} + \frac{d_n}{2b_n G_n}\right). \quad \text{(A1)}$$

Defining an average shear strain for the section $\bar{\gamma} = u/a = Q/S$ where $Q = t\kappa a$ and S are, respectively, the section shear force and stiffness, one obtains

$$S = Qa/u = t\kappa a^2/u. \quad \text{(A2)}$$

Using Eqs. (A1) and (A2) and taking $b = b_1 = \cdots = b_n$, one obtains Eq. (1).

References

[1] Ammer T, Brunauer A. Zollingers Rauten Neu Entdeckt (Discovering Zollinger's shells). Bauen mit Holz 1999;6:24–8. in German.
[2] Computers and Structures, Inc. (CSI). SAP 2000 (Version 7.12). Berkeley, CA, 2000.
[3] DIANA. Finite Element Analysis User's Manual Release 7.2. 3rd ed. The Netherlands: TNO Building and Construction Research, 1999.
[4] Forest Products Society (FPS). Wood handbook, Wood as an engineering material. [ISBN 1-892529-02-5], 1999.
[5] Gellert W, editor. Kleine Enzyklopädie Mathematik (Small mathematics encyclopedia). Leipzig, Germany: VEB Bibliographisches Institut; 1985. in German.
[6] German Code E DIN 1052. Entwurf, Berechnung und Bemessung von Holzbauwerken-Allgemeine Bemessungsregeln und Bemessungsregeln für den Hochbau. (Design and calculation for timber construction), May, 2000 (in German).
[7] Gliniorz KU, Hübner L. Tragverhalten von Brettstapelträgern (Design and experiments of multi-layer timber beams). Swiss Federal Institute of Technology Lausanne, Technical Report IBOIS 00:17, October, 2000 (in German).
[8] Heimeshoff B. Zur Berechnung von Biegeträgern aus Nachgiebig Miteinander Verbunden Querschnitten im Ingenieurbau (Computations of multi-layered beams under bending in timber construction). Holz als Roh- und Werkstoff 1987;6:237–41. in German.
[9] Kreuzinger H. Platten, Scheiben und Schalen-Ein Berechnungsmodell für Gängige Statikprogramme (Computational models for plates, walls, and beams). Bauen mit Holz 1999;1:34–9. in German.
[10] Möhler K. Über das Tragverhalten von Biegeträgern und Druckstützen mit Zusammengesetzten Querschnitten und Nachgiebigen Verbindungsmitteln (Overview of Computational Modeling of Multilayered Bending Beams and Columns). Habilitation Thesis. TU-Karlsruhe, 1956 (in German).
[11] Rots, JG. Computational modeling of concrete fracture. PhD Dissertation. Delft, The Netherlands: Delft University of Technology, 1988.